IEEE Access
Multidisciplinary | Rapid Review | Open Access Journal

Received December 1, 2019, accepted December 10, 2019, date of publication December 16, 2019,
date of current version December 31, 2019.

Digital Object Identifier 10.1109/ACCESS.2019.2960079

Fast Calculation of Scattering in Planar Uniaxial Anisotropic Multilayers

HUILING HU, HONGXIA YE, (Member, IEEE), AND YA-QIU JIN, (Fellow, IEEE)
Key Laboratory for Information Science of Electromagnetic Waves (MoE), Fudan University, Shanghai 200433, China

Corresponding author: Hongxia Ye (yehongxia@fudan.edu.cn)

This work was supported in part by the National Key Research and Development Program of China under Grant 2017YFB0502703, in part by the Natural Science Foundation of China under Grant 61991422, and in part by the National Natural Science Foundation of China under Grant 61871424.

ABSTRACT In this paper, the generalized recursive formulations of the finite difference time domain (FDTD) for updating the electric and magnetic fields in the multi-layer anisotropic media are derived with a uniaxial perfectly matched layer. The stability condition of the proposed method is clearly analyzed and verified. Then this method is used to calculate the three-dimensional complex scattering fields in planar multilayered anisotropic microstructures with optical axis perpendicular to the layered interface and the scattering fields of arbitrary shape scatters in the anisotropic layered structures. The electric field induced by the sine dipole source is calculated in the spatial domain and the corresponding spectral domain results are achieved through Fourier transform. The scattering field of composite materials with submillimeter thicknesses used in the industrial engineering is calculated using a terahertz wave with operation frequency of 0.3 THz. Robustness of the derived formulations for the complex uniaxial anisotropic media is verified by comparing with the COMSOL software, which is based on FEM analysis. The comparison of memory and CPU time shows the efficiency of the proposed FDTD method. Finally, the scattering fields of different scatters buried in multilayer anisotropic media are studied. So it is expected to become an effective simulation tool for dealing with complex electromagnetic environment in the future, such as abnormal detection of aircraft coating materials and detection of hidden target and so on.

INDEX TERMS Finite difference time domain, multilayers media, anisotropic, terahertz waves.

I. INTRODUCTION

The attraction of the subject of wave interaction in planar multilayered media stems from its relevance to many practical applications, ranging from geophysical exploration [1]–[3] to electromagnetic performance prediction of microwave antennas [4]–[5], aerospace industry applications [6]–[8], and microwave/millimeter wave integrated circuit (MMIC) wave guides [9]–[10]. With the continuous improvement of science and technology, the aerospace industry has constantly developed, and the performance and types of materials used are increasing. In striving for high corrosion resistance, sufficient stiffness and high strength-to-weight ratio, the aerospace industry has made the wide use of various composite materials. In particular, anisotropic composites have been widely used in civilian and defense applications for the aerospace industry in recent years.

The associate editor coordinating the review of this manuscript and approving it for publication was Lei Zhao.

The research methods of multilayer materials are also varied. Zhang Wen (2009) studied electromagnetic modeling and analysis for pulsed terahertz testing of hidden corrosion under aircraft coatings using the axisymmetrical form of Maxwell's equations and the finite element time domain (FETD) method, where the dispersion properties of the dielectrics were ignored [11]. In order to study the electromagnetic characteristics of planar multilayers of uniaxial media, Ping-Ping Ding et al. first derived the spatial-domain and spectral-domain dyadic Green's functions based on the modified fast Hankel transform (MFHT) method [12]. Yu Zhong et al. further proposed Padua point integration method to deal with the Sommerfeld integrals related to the dyadic Green's function for uniaxially anisotropic multilayers and studied the scattering problem of volume inhomogeneity in uniaxial planar layered media [13]. They used dyadic Green's functions in their eigen function expansion forms to analyze the planarly layered anisotropic media, which takes up a lot of memory because of the need for

matrix inversion. Therefore, the MoM method is much slower because of the calculation of Green's function.

The volume differential equation method, usually implemented via the finite difference time domain (FDTD), is a popular approach for many scattering problems, such as electromagnetic wave propagation in inhomogeneous anisotropic media. The FDTD method offers several advantages, such as robustness and the ability to study dispersive, nonlinear, or anisotropic materials. Moreover, the FDTD approach demonstrated excellent agreement with classic Mie scattering theory [14]. Since the differential equation solving process is simpler and can be used to analyze continuous electromagnetic problems, the FDTD method has been widely used for electromagnetic scattering of inhomogeneous bodies embedded within multi-layer media. In recent years, some researchers have used FDTD method to study layered media, which provides useful experience and knowledge for the study of multi-layer anisotropic media. For example, Schneider J. et al. derived the 3D FDTD formula for generalized anisotropic materials and calculated the electromagnetic field distribution and reflection coefficient in one-dimensional case [15]. However, it has not been applied to the case of three-dimensional multi-layer anisotropic media. Verdu J. B. et al. using FDTD method have studied the structures of different dielectric layers and transmission lines, but most of them are isotropic [16]. Sarto M. S. used full FDTD and hybrid MFIE/FDTD approaches to simulate composite multilayer plates [17]. Numerical applications to the analysis of the field distribution inside and outside a lightning struck aircraft are presented. But the method can not calculate the electromagnetic field distribution of micro-structure. Zhang H. et al. studied the shielding effectiveness (SE) high performance computing (HPC) of 3D multilayer anisotropic carbon fiber composite (CFC) thin layer [18]. Moss C.J et al. tried to study the numerical dispersion effects for the FDTD method in anisotropic and layered media [19], but he did give an explicit dispersion equation and numerical stability conditions.

Most of the abovementioned works are based on isotropic media, monolayer media, and 1D or 2D models. To the best of our knowledge, there are few theoretical studies on electromagnetic wave radiation propagation in anisotropic multilayered medium structures. In this paper, we extend the FDTD method to analyze 3D electromagnetic propagation of terahertz waves in anisotropic multilayered medium structures, and the electromagnetic scattering of embedded bodies. We chose terahertz wave because it has the advantages of the nonionization, the submillimeter resolution of observation images, and the relatively transparent nature of many materials to terahertz waves. THz inspection seems to be a very good choice for the examination of multilayered composites, such as detecting materials under coating layers [20]–[22] and characterizing layered polymer composites [23]–[24]. We calculate the propagation of THz waves in a multilayered uniaxial anisotropic medium. For the whole simulation domain, we derived a complete formulation for uniaxial anisotropic media. The electric field induced by the dipole source is calculated in the spatial domain and the spectral domain electric field is obtained through the Fourier transform. The proposed FDTD method could also be used as building block of an imaging procedure for damaged anisotropic laminates.

The main contributions of this paper are as follows:

1) We derive a generalized formulation for the entire simulation domain involving uniaxial anisotropic media and a perfectly matched layer absorbing boundary conditions.
2) We study anisotropic multilayered media and calculate the scattering field of terahertz wave in uniaxial multilayered microstructures.
3) Compared with the MoM method, which must calculate Green's function in, the scattering field can be solved directly and quickly.
4) FDTD simulations involving 3D-volumetric scatter with comparisons to finite element method (FEM) computations confirm the effectiveness of the approach and provide reliable benchmarks for further studies.

II. MODEL AND METHODS

As shown in Figure 1, the plane of the layered medium is at the plane. The sine dipole source will be set in any layer, on the interface of layered medium, or in the uppermost free space layer. When electromagnetic waves propagate in a multilayered medium, they will be reflected or transmitted wherever there is a sudden change in the refractive index or the optical absorption coefficient of the material (caused by either structural or chemical changes in the medium). In the following, the multilayered medium is set as an anisotropic medium, and the uniaxial perfectly matched layer (UPML) is used to derive the generalized 3D-FDTD formulas for both the uniaxial anisotropic model and the absorbing boundaries. These generalized equations can help to simplify numerical calculation process and significantly reduce the computational time.

The anisotropic Maxwell's curl equation in the case of a spectral-harmonic field is as follows.

$$\nabla \times \boldsymbol{H} = j\omega\,\bar{\boldsymbol{\varepsilon}} \cdot \boldsymbol{E} + \boldsymbol{J} \tag{1}$$

$$\nabla \times \boldsymbol{E} = -j\omega\,\bar{\boldsymbol{\mu}} \cdot \boldsymbol{H} \tag{2}$$

Here $\boldsymbol{H}$, $\boldsymbol{E}$, $\boldsymbol{J}$, $\bar{\boldsymbol{\varepsilon}}$, and $\bar{\boldsymbol{\mu}}$ are magnetic field, electric field, current density, permittivity and permeability, respectively. When we simultaneously consider the anisotropic UPML and the uniaxial medium models, the complex permittivity and the permeability can be written in tensor form as follows.

$$\bar{\boldsymbol{\varepsilon}} = \varepsilon_0 \bar{\boldsymbol{\varepsilon}}_r \bar{\boldsymbol{\varepsilon}}_p = \varepsilon_0 \begin{bmatrix} \varepsilon_x & 0 & 0 \\ 0 & \varepsilon_y & 0 \\ 0 & 0 & \varepsilon_z \end{bmatrix} \times \begin{bmatrix} \frac{s_y s_z}{s_x} & 0 & 0 \\ 0 & \frac{s_x s_z}{s_y} & 0 \\ 0 & 0 & \frac{s_y s_x}{s_z} \end{bmatrix} \tag{3}$$

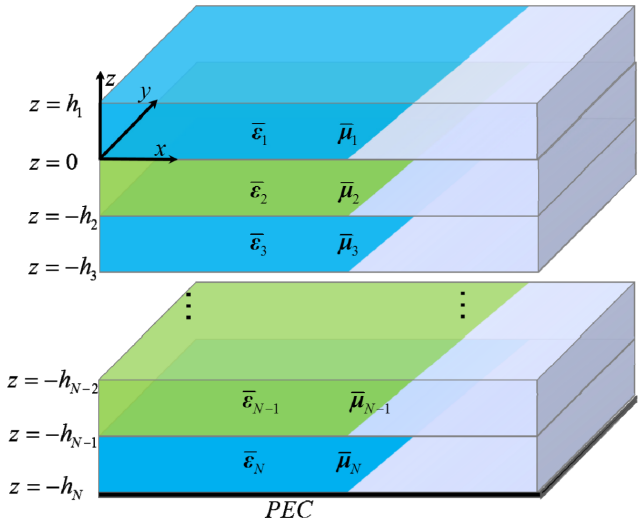

FIGURE 1. Theoretical model of the multilayered structure, where the lowermost layer is PEC.

$$\bar{\boldsymbol{\mu}} = \mu_0 \bar{\boldsymbol{\mu}}_r \bar{\boldsymbol{\mu}}_p = \mu_0 \begin{bmatrix} \mu_x & 0 & 0 \\ 0 & \mu_y & 0 \\ 0 & 0 & \mu_z \end{bmatrix} \times \begin{bmatrix} \frac{s_{y1}s_{z1}}{s_{x1}} & 0 & 0 \\ 0 & \frac{s_{x1}s_{z1}}{s_{y1}} & 0 \\ 0 & 0 & \frac{s_{y1}s_{x1}}{s_{z1}} \end{bmatrix} \tag{4}$$

Here, ε_0 and μ_0 are permittivity and permeability of the vacuum. $\bar{\boldsymbol{\varepsilon}}_r$ and $\bar{\boldsymbol{\mu}}_r$ are relative permittivity and permeability of the uniaxial medium model. $\bar{\boldsymbol{\varepsilon}}_p$ and $\bar{\boldsymbol{\mu}}_p$ are the matching matrices of permittivity and permeability of the anisotropic UPML model, respectively. At the same time, the matching relative permittivity and permeability are set as

$$s_i = 1 + \frac{\sigma_i}{j\omega\varepsilon_0} \ (i = x, y, z) \tag{5}$$

$$s_{i1} = 1 + \frac{\rho_i}{j\omega\varepsilon_0} \ (i = x, y, z) \tag{6}$$

where σ_i and ρ_i are conductivity and reluctivity along the i-axis, respectively.

According to the constitutive relation of electromagnetic medium, the generalized 3D coupling equations in time domain can be derived with (1) and (2). Taking the equation in x-direction as an example, the renewal equations are derived as

$$\frac{\partial H_z}{\partial y} - \frac{\partial H_y}{\partial z} = \frac{\partial D_x}{\partial t} + \frac{\sigma_y}{\varepsilon_0} D_x + J_x \tag{7}$$

$$\frac{\partial D_x}{\partial t} + \frac{\sigma_x}{\varepsilon_0} D_x = \varepsilon_0 \varepsilon_x \frac{\partial E_x}{\partial t} + \varepsilon_x \sigma_z E_x \tag{8}$$

$$\frac{\partial E_z}{\partial y} - \frac{\partial E_y}{\partial z} = -\frac{\partial B_x}{\partial t} - \frac{\rho_y}{\varepsilon_0} B_x \tag{9}$$

$$\frac{\partial B_x}{\partial t} + \frac{\rho_x}{\varepsilon_0} B_x = \mu_0 \mu_x \frac{\partial H_x}{\partial t} + \frac{\mu_0 \mu_x}{\varepsilon_0} \rho_z H_x \tag{10}$$

Here $\boldsymbol{D}$ and $\boldsymbol{B}$ are intermediate variables related to the electric and magnetic flux density, and defined as

$$D_x = \varepsilon_0 \varepsilon_x \frac{s_z}{s_x} E_x, D_y = \varepsilon_0 \varepsilon_y \frac{s_x}{s_y} E_y, D_z = \varepsilon_0 \varepsilon_z \frac{s_y}{s_z} E_z \tag{11}$$

$$B_x = \mu_0 \mu_x \frac{s_{z1}}{s_{x1}} H_x, B_y = \mu_0 \mu_y \frac{s_{x1}}{s_{y1}} H_y, B_z = \mu_0 \mu_z \frac{s_{y1}}{s_{z1}} H_z \tag{12}$$

Following Yee's rules, any function of space and time is discretized as

$$F^n(i, j, k) = F\left(i\Delta_x, j\Delta_y, k\Delta_z, n\Delta_t\right) \tag{13}$$

where Δ_x, Δ_y and Δ_z are the space increments and Δ_t is the time increment. To facilitate the FDTD iteration, we stipulate flux density components $\boldsymbol{D}$ and the electric field components $\vec{E}$ at integer time steps, i.e., $\boldsymbol{E}^n$ and $\boldsymbol{D}^n$, $\boldsymbol{H}$ and $\boldsymbol{B}$ at half time steps, i.e., $\boldsymbol{H}^{n+1/2}$ and $\boldsymbol{B}^{n+1/2}$. Then (7-10) can be discretized into iterative forms. Taking x-direction as an example, the iterative equations can be obtained as

$$\begin{aligned} &D_x^n\left(i+\frac{1}{2}, j, k\right) = \\ &\frac{2\varepsilon_0 - \Delta_t\sigma_y\left(i+\frac{1}{2}, j, k\right)}{2\varepsilon_0 + \Delta_t\sigma_y\left(i+\frac{1}{2}, j, k\right)} \cdot D_x^{n-1}\left(i+\frac{1}{2}, j, k\right) \\ &- \frac{2\varepsilon_0\Delta_t}{2\varepsilon_0 + \Delta_t\sigma_y\left(i+\frac{1}{2}, j, k\right)} \cdot J_x^{n-\frac{1}{2}}\left(i+\frac{1}{2}, j, k\right) \\ &+ \frac{2\varepsilon_0\Delta_t}{2\varepsilon_0 + \Delta_t\sigma_y\left(i+\frac{1}{2}, j, k\right)} \\ &\cdot \left[\frac{H_z^{n-\frac{1}{2}}\left(i+\frac{1}{2}, j+\frac{1}{2}, k\right) - H_z^{n-\frac{1}{2}}\left(i+\frac{1}{2}, j-\frac{1}{2}, k\right)}{\Delta_y}\right. \\ &\left. - \frac{H_y^{n-\frac{1}{2}}\left(i+\frac{1}{2}, j, k+\frac{1}{2}\right) - H_y^{n-\frac{1}{2}}\left(i+\frac{1}{2}, j, k-\frac{1}{2}\right)}{\Delta_z}\right] \end{aligned} \tag{14}$$

$$\begin{aligned} &E_x^n\left(i+\frac{1}{2}, j, k\right) = \\ &\frac{2\varepsilon_0 - \Delta_t\sigma_z\left(i+\frac{1}{2}, j, k\right)}{2\varepsilon_0 + \Delta_t\sigma_z\left(i+\frac{1}{2}, j, k\right)} \cdot E_x^{n-1}\left(i+\frac{1}{2}, j, k\right) \\ &+ \frac{2\varepsilon_0 + \Delta_t\sigma_x\left(i+\frac{1}{2}, j, k\right)}{2\varepsilon_0^2\varepsilon_x + \Delta_t\varepsilon_0\varepsilon_x\sigma_z\left(i+\frac{1}{2}, j, k\right)} \cdot D_x^n\left(i+\frac{1}{2}, j, k\right) \\ &- \frac{2\varepsilon_0 - \Delta_t\sigma_x\left(i+\frac{1}{2}, j, k\right)}{2\varepsilon_0^2\varepsilon_x + \Delta_t\varepsilon_0\varepsilon_x\sigma_z\left(i+\frac{1}{2}, j, k\right)} \cdot D_x^{n-1}\left(i+\frac{1}{2}, j, k\right) \end{aligned} \tag{15}$$

$$B_x^{n+\frac{1}{2}}\left(i,j+\frac{1}{2},k+\frac{1}{2}\right)=$$
$$\frac{2\varepsilon_0-\Delta_t\rho_y\left(i,j+\frac{1}{2},k+\frac{1}{2}\right)}{2\varepsilon_0+\Delta_t\rho_y\left(i,j+\frac{1}{2},k+\frac{1}{2}\right)}\cdot B_x^{n-\frac{1}{2}}\left(i,j+\frac{1}{2},k+\frac{1}{2}\right)$$
$$-\frac{1}{2\varepsilon_0+\Delta_t\rho_y\left(i,j+\frac{1}{2},k+\frac{1}{2}\right)}$$
$$\cdot\left[\frac{E_z^n\left(i,j+1,k+\frac{1}{2}\right)-E_z^n\left(i,j,k+\frac{1}{2}\right)}{\Delta_y}\right.$$
$$\left.-\frac{E_y^n\left(i,j+\frac{1}{2},k+1\right)-E_y^n\left(i,j+\frac{1}{2},k\right)}{\Delta_z}\right] \quad (16)$$

$$H_x^{n+\frac{1}{2}}\left(i,j+\frac{1}{2},k+\frac{1}{2}\right)=$$
$$\frac{2\varepsilon_0-\Delta_t\rho_z\left(i,j+\frac{1}{2},k+\frac{1}{2}\right)}{2\varepsilon_0+\Delta_t\rho_z\left(i,j+\frac{1}{2},k+\frac{1}{2}\right)}\cdot H_x^{n-\frac{1}{2}}\left(i,j+\frac{1}{2},k+\frac{1}{2}\right)$$
$$+\frac{2\varepsilon_0+\Delta_t\rho_x\left(i,j+\frac{1}{2},k+\frac{1}{2}\right)}{2\varepsilon_0\mu_0\mu_x+\Delta_t\mu_0\mu_x\rho_z\left(i,j+\frac{1}{2},k+\frac{1}{2}\right)}$$
$$\cdot B_x^{n+\frac{1}{2}}\left(i,j+\frac{1}{2},k+\frac{1}{2}\right)$$
$$-\frac{2\varepsilon_0-\Delta_t\rho_x\left(i,j+\frac{1}{2},k+\frac{1}{2}\right)}{2\varepsilon_0\mu_0\mu_x+\Delta_t\mu_0\mu_x\rho_z\left(i,j+\frac{1}{2},k+\frac{1}{2}\right)}$$
$$\cdot B_x^{n-\frac{1}{2}}\left(i,j+\frac{1}{2},k+\frac{1}{2}\right) \quad (17)$$

Other y and z component formulae can be derived via a similar procedure as shown in the Appendix. Then, the time update progression sequence is expressed as $\boldsymbol{H}^{n-1/2} \rightarrow \boldsymbol{D}^n \rightarrow \boldsymbol{E}^n \rightarrow \boldsymbol{B}^{n+1/2} \rightarrow \boldsymbol{H}^{n+1/2}$.

In this paper, the UPML absorbing boundaries are chosen to mimic the unbounded space. Considering the anisotropic characteristics of the uniaxial multi-layer structures, four layers of UPML are utilized to maximally absorbing the out-going waves. To simply the settings, the ideal conductor is put as the outermost truncation boundary of PML. For each layer, the conductivity σ_i and reluctivity ρ_i of each axis are non-uniform stratification. Take the interface perpendicular to x-axis as an example, the transverse conductivities $\sigma_y = \sigma_z = 0$ and σ_x is only related to x as [25]

$$\sigma_x(x)=\frac{\sigma_{\max}|x-x_0|^m}{d^m} \quad (18)$$

where d is the total thickness of PML layer, x_0 is the interface position of PML layer near FDTD area. m is the layer number, and is valued as $m = 4$ in this paper. The conductivity reaches maximum at the outermost layer, and the best value is chose as

$$\sigma_{\max}=(m+1)/\left(150\pi\Delta_x\sqrt{\varepsilon_{\min}}\right) \quad (19)$$

where Δ_x is space step along x-axis. As can be seen from (19), the value of $\sigma_{\max}$ will be different for each layer of the multilayer medium. Parameters of PML layer alone y-axis and z-axis can be set similarly.

III. NUMERICAL DISPERSION RELATION FOR ANISOTROPIC UNIAXIAL MEDIA

We consider a time harmonic form $V^n(i,j,k) = Ve^{j_0(ik_x\Delta_x+jk_y\Delta_y+kk_z\Delta_z-n\omega\Delta_t)}$ for each component of electromagnetic field. Here j_0 is the imaginary unit, and (k_x, k_y, k_z) are the three components of the incident wave vector, and ω is the angular frequency of the incident electromagnetic. By applying this form to (7-10), we obtain the following eigen matrix.

$$\Delta=\begin{bmatrix} C_1 & \tilde{\partial}_x\hat{\partial}_y & \tilde{\partial}_x\hat{\partial}_z \\ \tilde{\partial}_y\hat{\partial}_x & C_2 & \tilde{\partial}_y\hat{\partial}_z \\ \tilde{\partial}_z\hat{\partial}_x & \tilde{\partial}_z\hat{\partial}_y & C_3 \end{bmatrix} \quad (20)$$

Here $\tilde{\partial}$ denotes the forward difference operator and $\hat{\partial}$ denotes the backward difference operator, whose expressions were given in Ref. [24]. After setting the determinant of the matrix in (20) to zero, we can get the eigenvalue equation. For an anisotropic uniaxial media with low conductivity, the algebraic equation is

$$-\mu^2\varepsilon_z\varepsilon_x^2\lambda^4+\mu\left\{(\varepsilon_x+\varepsilon_z)\varepsilon_x[X+Y]+2\varepsilon_x\varepsilon_z Z\right\}\lambda^2$$
$$-\varepsilon_x\left[Y^2+X^2\right]-\varepsilon_z Z^2-(\varepsilon_x+\varepsilon_z)Z[X+Y]-2\varepsilon_x^2 Y=0 \quad (21)$$

Here,

$$X=\frac{\sin^2\left(k_x\frac{\Delta_x}{2}\right)}{\left(\frac{\Delta_x}{2}\right)^2},\ Y=\frac{\sin^2\left(k_y\frac{\Delta_y}{2}\right)}{\left(\Delta_y\right)^2},\ Z=\frac{\sin^2\left(k_z\frac{\Delta_z}{2}\right)}{\left(\frac{\Delta_z}{2}\right)^2} \quad (22)$$

The solution of (21) is

$$\lambda^2=-\frac{X+Y+Z}{\mu\varepsilon_x} \quad (23)$$
$$\lambda^2=-\frac{\varepsilon_x(X+Y)+\varepsilon_z Z}{\mu\varepsilon_x\varepsilon_z} \quad (24)$$

In order to satisfy the stability condition for all possible k_x, k_y, k_z the time dispersion must satisfy the following conditions

$$\Delta_t\le\frac{1}{\sqrt{\mu\max(\varepsilon_x,\varepsilon_z)}\sqrt{\frac{1}{(\Delta_x)^2}+\frac{1}{(\Delta_y)^2}+\frac{1}{(\Delta_z)^2}}} \quad (25)$$

In the following numerical simulation, the discrete step size of time and space needs to satisfy (25) for each layer.

IV. NUMERICAL EXAMPLES

A. LOSSLESS ANISOTROPIC UNIAXIAL MEDIA

We use the above generalized equations to calculate the scattered field of scatters buried in the three-dimensional planar uniaxial anisotropic multilayer, where the lowermost layer is PEC. Perfect multilayered materials and defective multilayered materials are within our consideration. The calculation results of the first two examples are compared with the outcome obtained by COMSOL (a software based on the

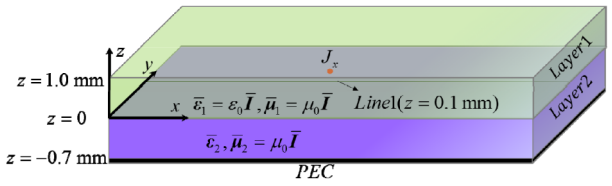

FIGURE 2. Geometry of the perfect two-layer uniaxial anisotropic structure.

finite element method) to verify the accuracy of the numerical results. The latter two examples are used to study the complex scattering fields of more complex scatters buried in multilayered anisotropic media. These results will help to detect abnormal damage in aircraft coating structure. In the following numerical examples, the operating frequency is 0.3 THz.

Composite material is any new material that is optimized by advanced material preparation technology. The purpose of composite preparation is to meet the needs of certain functions. Therefore, it is meaningful to study the distribution of the internal field of composite materials with specific sources. The first example is a two-layer geometric structure, as shown in Figure 2. With $\bar{\boldsymbol{I}}$ as the identity tensor, the permittivity of layer 1 is $\bar{\boldsymbol{\varepsilon}}_1 = \varepsilon_0\bar{\boldsymbol{I}}$. Along the principal axes, the permittivity of layer 2 is $\bar{\boldsymbol{\varepsilon}}_2 = diag\,[2.1, 2.1, 4.2]\,\varepsilon_0$. A sine wave dipole source is set for J_x at point P(4 mm, 0.5 mm, 0.2 mm) inside layer 1, as shown in Figure 2. *Line*1 ($y = 0.5$ mm , $z = 0.1$ mm) is chosen as the monitoring line. Here, according to the stability condition, we get a space interval of 5 nm and a time interval of $8.3333 \times 10^{-14}s$.

The above FDTD method is used for numerical simulation and the UPML is used to absorb outward electromagnetic waves without reflection, so that the infinite propagation space can be truncated into a limited area for numerical simulation. For the simulation domain, the transverse dimension in XY plane is 8.0 mm × 1.0 mm. The thickness of the first layer along the z-direction is 1 mm, and the thickness of the second layer is 0.7 mm. Thus, the computational domain is discretized into $180 \times 40 \times 44$ mesh grids. Figure 3 shows the magnitude of the electric field E_x and E_z along line 1. The results show that the error between our FDTD method and the COMSOL software is less than 0.2 dB, which shows that the results are in good agreement and proves the validity of the method. We used the same PC machine with main frequency of 3.2 GHz. Our FDTD method FDTD method takes 6 minutes, while COMSOL software takes 12 minutes, thus demonstrating the efficiency of our FDTD method.

The multilayer structure is often used in engineering such as aircraft coatings and radomes. Although the manufacturing technology of composite materials has been greatly improved with the progress of science and technology, there is still some unavoidable faultiness in the preparation and use of composite materials. For example, other characteristic inclusions are mixed during the material manufacturing process, air bubbles exist in the material, and cracks or peeling problems occur in

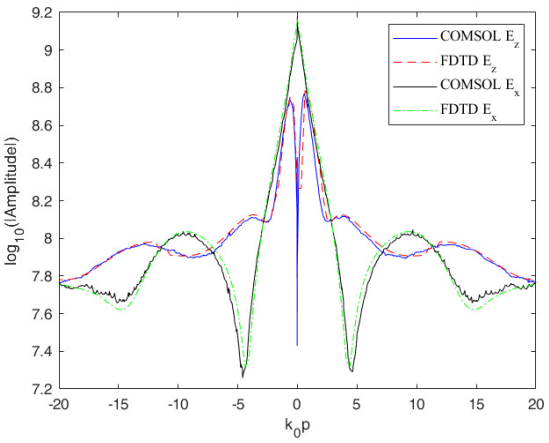

FIGURE 3. Electric fields along line 1.

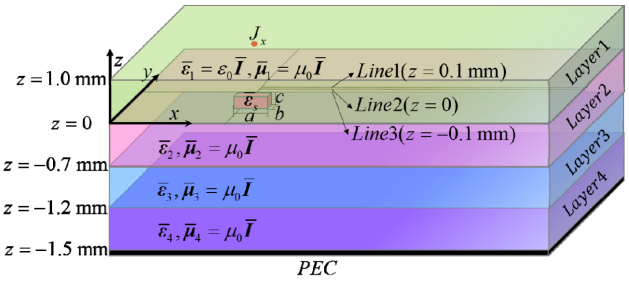

FIGURE 4. Geometry of the four-layer uniaxial anisotropic structure with an air inclusion scatter.

the material. In the following examples, we try to calculate the scattering fields due to some scatters of different shapes in multilayer structures.

In the following three examples shown in Figure 4, 6 and 8, the basic structure and parameters of the multilayered material are the same as a four-layer uniaxial anisotropic structure where the uppermost layer is taken to be free space, while the lowermost layer is PEC. With $\bar{\boldsymbol{I}}$ as the identity tensor, the permittivity of layer 1 is $\bar{\boldsymbol{\varepsilon}}_1 = \varepsilon_0\bar{\boldsymbol{I}}$. The second to fourth layers are uniaxial anisotropic media. Along their principal axes, the permittivity are $\bar{\boldsymbol{\varepsilon}}_2 = diag\,[2.1, 2.1, 4.2]\,\varepsilon_0$, $\bar{\boldsymbol{\varepsilon}}_3 = diag\,[9.8, 9.8, 19.6]\,\varepsilon_0$, and $\bar{\boldsymbol{\varepsilon}}_4 = diag\,[8.6, 8.6, 17.2]\,\varepsilon_0$, respectively. The thicknesses along the z-direction are 1.0 mm, 0.7 mm, 0.55 mm and 0.3 mm, respectively. A sine wave dipole source is set for J_x at point P (4 mm, 0.5 mm, 0.2 mm) inside the free space layer (layer 1).

In these simulation, ''case 1'' represents the scattering field when only anisotropic materials exist (total scattering field generated by ''media'' minus incident scattering field generated by ''air''), ''case 2'' represents the scattering field when there are anisotropic materials and scatters (total scattering field generated by ''media + scatter'' minus incident scattering field generated by ''air''), and ''case 3'' represents the scattering field generated by the scatter (scattering field generated by ''media + scatter'' minus scattering field generated by ''media'').

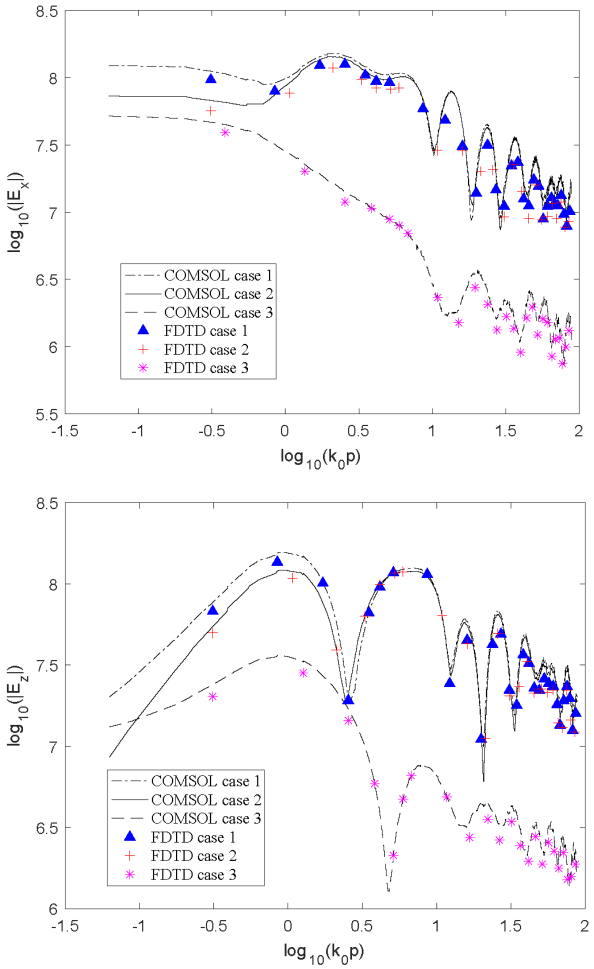

FIGURE 5. Scattered electric fields E_x and E_z along line1.

The first example as shown in Figure 4 involves a parallelepiped air inclusion (its permittivity is $\bar{\boldsymbol{\varepsilon}}_s = \varepsilon_0 \bar{\boldsymbol{I}}$, and it size is $4 \times 4 \times 4$ mesh) embedded in the second layer, which is also a type of normal defect in composite materials. Its upper surface is located at $z = -0.1$ mm and its horizontal position is in the middle. The lateral dimension of simulation area in Figure 4 is $x \times y = 16.0$ mm $\times$ 2.0 mm. The whole computational domain is discrete into $340 \times 60 \times 60$ mesh grids.

Figure 5 shows the x-component and z-component of the scattered electric field along *Line*1 ($z = 0.1$ mm). It is evident from the resultant plots that the spectral-domain electric fields obtained by this example agree very well with the multi-physics COMSOL software based on the finite element method. We used the same 3.2-GHz PC to run this numerical experiment. Compared with the computational time and memory occupied by COMSOL software, the FDTD method calculates the scattering field of uniaxial planar layered media in a shorter time and occupies less memory. In terms of computational time, using COMSOL software to calculate case 1, case 2 and case 3 takes 185 minutes, 191 minutes and 312 minutes respectively, while FDTD method takes

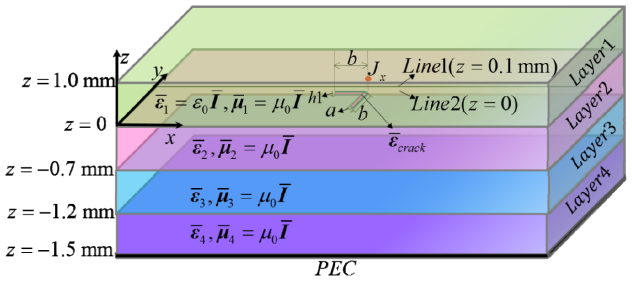

FIGURE 6. Geometry of the four-layer uniaxial anisotropic structure with one right-angle crack.

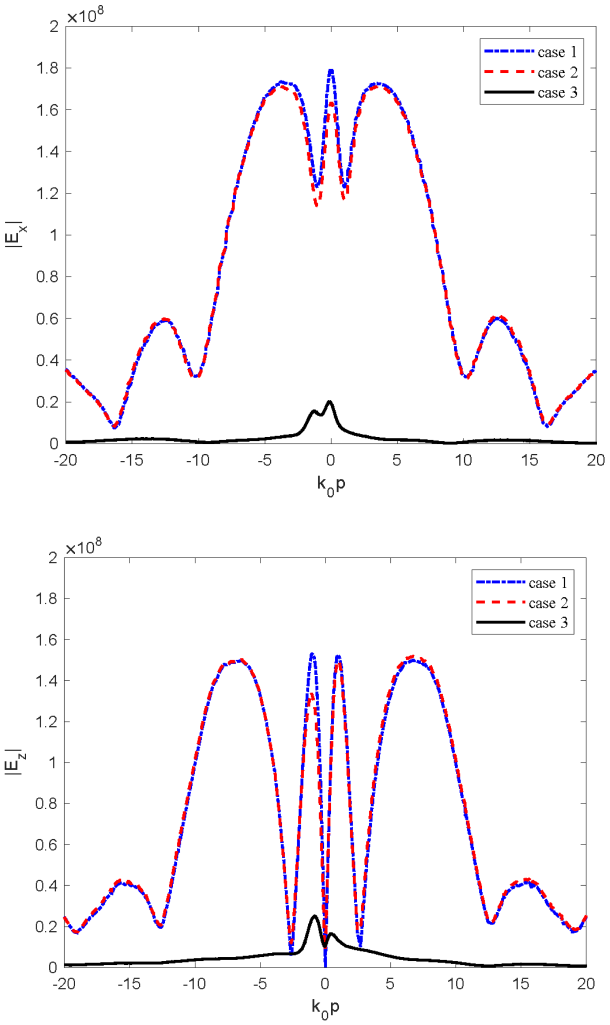

FIGURE 7. Scattered electric fields E_x and E_z along line1.

65 minutes, 64 minutes and 63 minutes respectively. In terms of memory occupied, FDTD method occupies 1.42 GB, but COMSOL method has reached 109.6 GB. So this FDTD method is suitable for complex scattering problems.

The second example as shown in Figure 6 involves a right-angled crack with only one grid width on the surface of the second layer. The size parallel to x-axis is 0.3 mm $\times$ 0.05 mm $\times$ 0.1 mm, and the other size parallel to y-axis is 0.05 mm $\times$ 0.3 mm $\times$ 0.1 mm. The crack is filled with air

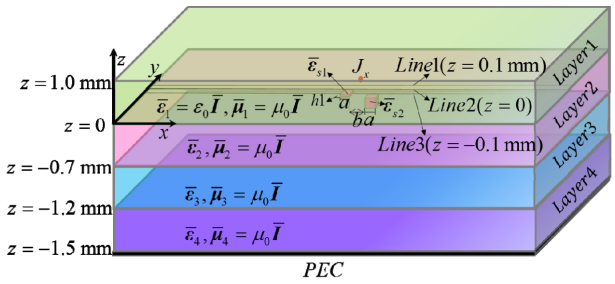

FIGURE 8. Geometry of the four-layer uniaxial anisotropic structure with two scatters.

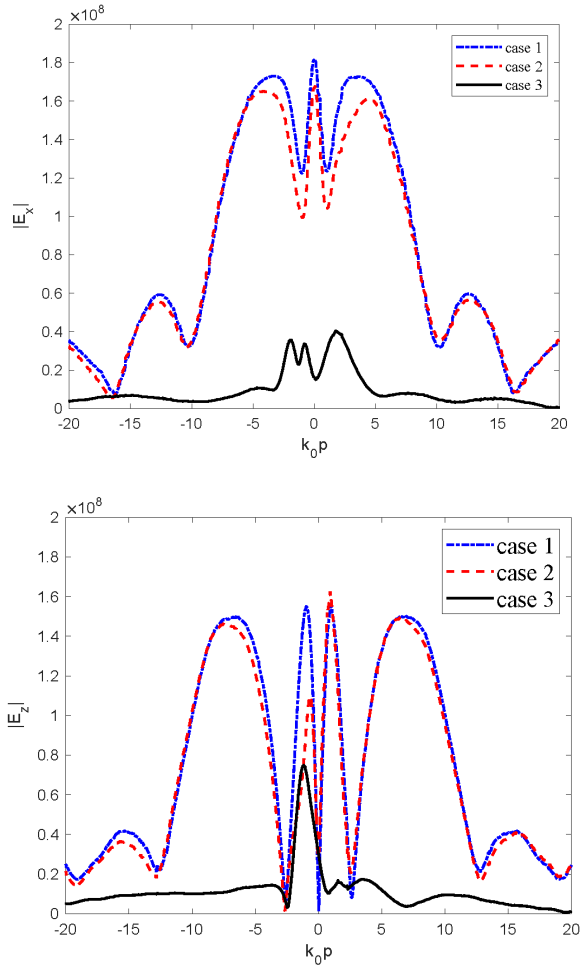

FIGURE 9. Scattered electric fields E_x and E_z along line1.

($\bar{\boldsymbol{\varepsilon}}_{crack} = \varepsilon_0\bar{\boldsymbol{I}}$), and its upper surface is at $z = 0$. In this example, the source is at $(x/2, y/2, 0)$. The monitoring line is at *Line*1 ($z = 0.1$ mm). Figure 7 shows the magnitude of the scattered electric field E_x and E_z as a function of the horizontal distance from the source alone line 1.

The third example as shown in Figure 8 involves two parallel hexahedron scatters embedded in the second layer. One is an air inclusion of size 0.2 mm × 0.2 mm × 0.1 mm, where the upper surface of the air inclusion is located at the interface of the first layer and the second layer, and its permittivity is $\bar{\boldsymbol{\varepsilon}}_{s1} = \varepsilon_0\bar{\boldsymbol{I}}$. The other one is a cubic uniaxial medium

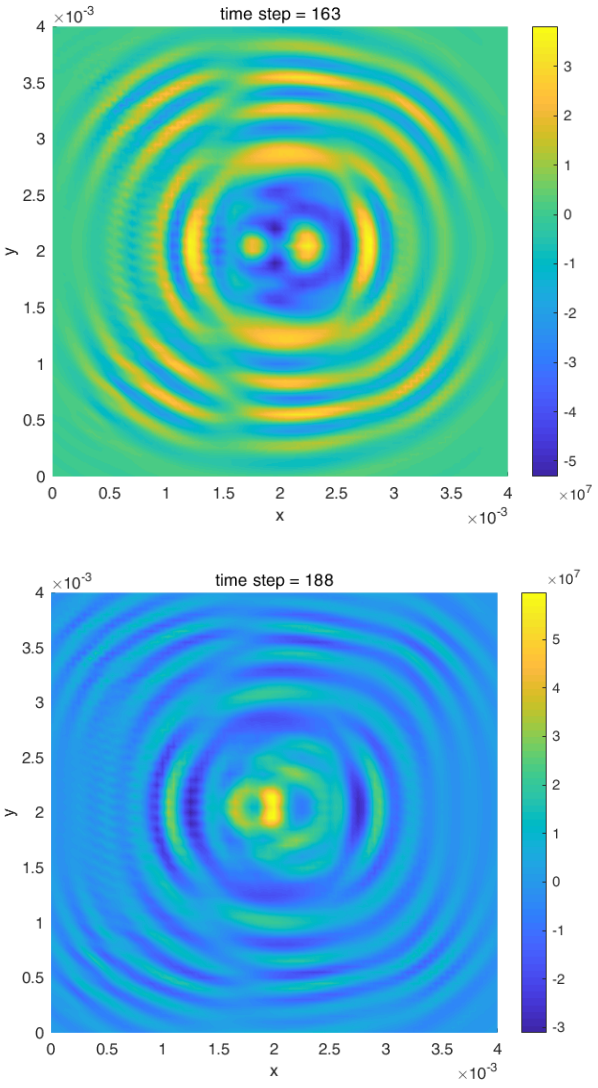

FIGURE 10. Distribution of the scattered time-domain electric field E_x in the XY plane at $z = 0.1$ mm.

inclusion with side length of 0.2 mm and permittivity of $\bar{\boldsymbol{\varepsilon}}_{s2} = diag\,[1, 1, 2]\,\varepsilon_0$. Its upper surface is located at $z =$ - 0.1mm. The horizontal distance between the two scatters in the x-direction is 0.25 mm. The monitoring line is at *Line*1 ($z =$ 0.1 mm). The source location in this example is the same as above. Figure 9 shows the magnitude of the scattered electric field E_x and E_z as a function of the horizontal distance from the source.

The distribution of the scattered field in the time domain directly indicates the wave propagation in the complicated anisotropic media, including the global reflection and global transmission in the multilayered structure. Figure 10 shows the time-domain electric fields in the xy plane at the time step 163 and 188, respectively. The position at z direction is $z = 0.1$ mm. It can be seen that the scattered field is strongly influenced by two scatters which are very close to each other. The influenced scattered field due to the left scatter is much smaller than that due to the right scatter. These phenomena are consistent with the actual geometry structure.

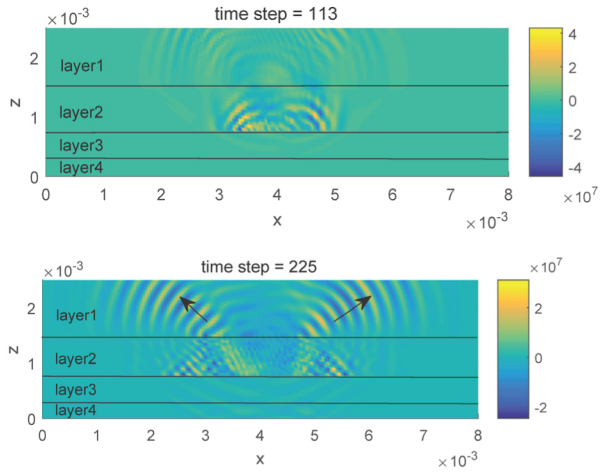

FIGURE 11. Distribution of the scattered time-domain electric field E_x in the XZ plane at $y = 0.9$ mm.

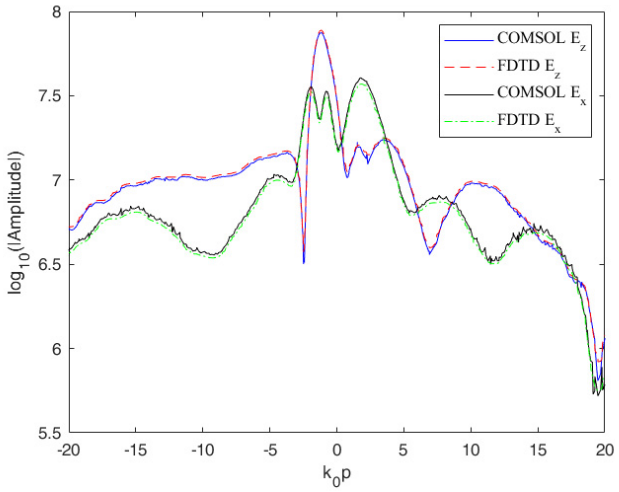

FIGURE 12. Scattered electric fields E_x and E_z along line1 in Figure 8.

Figure 11 shows the scattered time-domain field in the xz plane at $y = 0.9$ mm. The two subfigures at different time steps obviously demonstrate the complicated wave propagation in the multilayered structure. The global reflections and transmissions can be seen and numerically recorded in a straight way by our method.

B. LOSSY ANISOTROPIC UNIAXIAL MEDIA

The algorithm is extended and tested on a lossy anisotropic uniaxial media problem. Because of the global character of the algorithm, it is very simple to expand from lossless medium to lossy medium. To test its applicability, the propagation of scattering field generated by dipole source in anisotropic uniaxial medium with low conductivity is studied. In this example, we use the same model as Figure 8 to calculate the scattering field, except that the parameters of each layer are different. And the operating frequency is also 0.3 THz. Layer 1 of the computational domain is air. The second to fourth layers are low loss uniaxial anisotropic media. Along their principal axes, the permittivity are $\bar{\boldsymbol{\varepsilon}}_2 = diag\,[2.1, 2.1, 4.2]\,\varepsilon_0$, $\bar{\boldsymbol{\varepsilon}}_3 = diag\,[9.8, 9.8, 19.6]\,\varepsilon_0$, and $\bar{\boldsymbol{\varepsilon}}_4 = diag\,[8.6, 8.6, 17.2]\,\varepsilon_0$. The conductivity are $\bar{\boldsymbol{\sigma}}_2 = 0.0001 \times diag\,[1, 1, 2]$, $\bar{\boldsymbol{\sigma}}_3 = 0.0001 \times diag\,[2, 2, 4]$ and $\bar{\boldsymbol{\sigma}}_4 = 0.0001 \times diag\,[2.5, 2.5, 5]$. The source location in this example is the same as above. Figure 12 shows the magnitude of the scattered electric fields E_x and E_z as a function of the horizontal distance from the source. It can be seen from the result chart that our method can also get better results under the condition of low loss and conductivity.

V. CONCLUSION

In this paper, scattering by microstructural volumetric inhomogeneity in uniaxial planar multilayered media with optical axes perpendicular to the layer interface was calculated. The FDTD method is utilized, and the generalized formulations are derived with a uniaxial perfectly matched layer. The stability condition is given to restrict the time and spatial steps for updating the recursive equations. A Fourier transform is used to derive the scattered field value in the frequency domain. Based on the FDTD method, fast scattering solutions are obtained for the multilayered uniaxial anisotropic media. Numerical simulations involving uniaxial multilayered media, when compared to results provided by COMSOL software based on the finite element method, show that the three-dimensional finite difference method can produce accurate results in an efficient fashion. Moreover, the global reflections and transmissions can be seen and numerically recorded in a straight way by this method, which can be used as a reliable benchmark for further research.

APPENDIX

The FDTD difference formula in y-direction is derived as

$$
\begin{aligned}
&D_y^n\left(i, j+\frac{1}{2}, k\right) = \\
&\frac{2\varepsilon_0 - \Delta_t\sigma_z\left(i, j+\frac{1}{2}, k\right)}{2\varepsilon_0 + \Delta_t\sigma_z\left(i, j+\frac{1}{2}, k\right)} \cdot D_y^{n-1}\left(i, j+\frac{1}{2}, k\right) \\
&-\frac{2\varepsilon_0\Delta_t}{2\varepsilon_0 + \Delta_t\sigma_z\left(i, j+\frac{1}{2}, k\right)} \cdot J_y^{n-\frac{1}{2}}\left(i, j+\frac{1}{2}, k\right) \\
&+\frac{2\varepsilon_0\Delta_t}{2\varepsilon_0 + \Delta_t\sigma_z\left(i, j+\frac{1}{2}, k\right)} \\
&\cdot\left[\frac{H_x^{n-\frac{1}{2}}\left(i, j+\frac{1}{2}, k+\frac{1}{2}\right) - H_x^{n-\frac{1}{2}}\left(i, j+\frac{1}{2}, k-\frac{1}{2}\right)}{\Delta_z}\right. \\
&\left.-\frac{H_z^{n-\frac{1}{2}}\left(i+\frac{1}{2}, j+\frac{1}{2}, k\right) - H_z^{n-\frac{1}{2}}\left(i-\frac{1}{2}, j+\frac{1}{2}, k\right)}{\Delta_x}\right]
\end{aligned}
\tag{A1}
$$

$$
\begin{aligned}
&E_y^n\left(i, j+\frac{1}{2}, k\right) = \\
&\frac{2\varepsilon_0 - \Delta_t\sigma_x\left(i, j+\frac{1}{2}, k\right)}{2\varepsilon_0 + \Delta_t\sigma_x\left(i, j+\frac{1}{2}, k\right)} \cdot E_y^{n-1}\left(i, j+\frac{1}{2}, k\right)
\end{aligned}
$$

$$+\frac{2\varepsilon_0+\Delta_t\sigma_y\left(i,j+\frac{1}{2},k\right)}{2\varepsilon_0^2\varepsilon_y+\Delta_t\varepsilon_0\varepsilon_y\sigma_x\left(i,j+\frac{1}{2},k\right)}\cdot D_y^n\left(i,j+\frac{1}{2},k\right)$$
$$-\frac{2\varepsilon_0-\Delta_t\sigma_y\left(i,j+\frac{1}{2},k\right)}{2\varepsilon_0^2\varepsilon_y+\Delta_t\varepsilon_0\varepsilon_y\sigma_x\left(i,j+\frac{1}{2},k\right)}\cdot D_y^{n-1}\left(i,j+\frac{1}{2},k\right) \tag{A2}$$

$$B_y^{n+\frac{1}{2}}\left(i+\frac{1}{2},j,k+\frac{1}{2}\right)=$$
$$\frac{2\varepsilon_0-\Delta_t\rho_z\left(i+\frac{1}{2},j,k+\frac{1}{2}\right)}{2\varepsilon_0+\Delta_t\rho_z\left(i+\frac{1}{2},j,k+\frac{1}{2}\right)}\cdot B_y^{n-\frac{1}{2}}\left(i+\frac{1}{2},j,k+\frac{1}{2}\right)$$
$$-\frac{1}{2\varepsilon_0+\Delta_t\rho_z\left(i+\frac{1}{2},j,k+\frac{1}{2}\right)}$$
$$\cdot\left[\frac{E_x^n\left(i+\frac{1}{2},j,k+1\right)-E_x^n\left(i+\frac{1}{2},j,k\right)}{\Delta_z}\right.$$
$$\left.-\frac{E_z^n\left(i+1,j,k+\frac{1}{2}\right)-E_z^n\left(i,j,k+\frac{1}{2}\right)}{\Delta_x}\right] \tag{A3}$$

$$H_y^{n+\frac{1}{2}}\left(i+\frac{1}{2},j,k+\frac{1}{2}\right)=$$
$$\frac{2\varepsilon_0-\Delta_t\rho_x\left(i+\frac{1}{2},j,k+\frac{1}{2}\right)}{2\varepsilon_0+\Delta_t\rho_x\left(i+\frac{1}{2},j,k+\frac{1}{2}\right)}\cdot H_y^{n-\frac{1}{2}}\left(i+\frac{1}{2},j,k+\frac{1}{2}\right)$$
$$+\frac{2\varepsilon_0+\Delta_t\rho_y\left(i+\frac{1}{2},j,k+\frac{1}{2}\right)}{2\varepsilon_0\mu_0\mu_y+\Delta_t\mu_0\mu_y\rho_x\left(i+\frac{1}{2},j,k+\frac{1}{2}\right)}$$
$$\cdot B_y^{n+\frac{1}{2}}\left(i+\frac{1}{2},j,k+\frac{1}{2}\right)$$
$$-\frac{2\varepsilon_0-\Delta_t\rho_y\left(i+\frac{1}{2},j,k+\frac{1}{2}\right)}{2\varepsilon_0\mu_0\mu_y+\Delta_t\mu_0\mu_y\rho_x\left(i+\frac{1}{2},j,k+\frac{1}{2}\right)}$$
$$\cdot B_y^{n-\frac{1}{2}}\left(i+\frac{1}{2},j,k+\frac{1}{2}\right) \tag{A4}$$

The FDTD difference formula in z-direction is derived as

$$D_z^n\left(i,j,k+\frac{1}{2}\right)=$$
$$\frac{2\varepsilon_0-\Delta_t\sigma_x\left(i,j,k+\frac{1}{2}\right)}{2\varepsilon_0+\Delta_t\sigma_x\left(i,j,k+\frac{1}{2}\right)}\cdot D_z^{n-1}\left(i,j,k+\frac{1}{2}\right)$$
$$-\frac{2\varepsilon_0\Delta_t}{2\varepsilon_0+\Delta_t\sigma_x\left(i,j,k+\frac{1}{2}\right)}\cdot J_z^{n-\frac{1}{2}}\left(i,j,k+\frac{1}{2}\right)$$
$$+\frac{2\varepsilon_0\Delta_t}{2\varepsilon_0+\Delta_t\sigma_x\left(i,j,k+\frac{1}{2}\right)}$$
$$\cdot\left[\frac{H_y^{n-\frac{1}{2}}\left(i+\frac{1}{2},j,k+\frac{1}{2}\right)-H_y^{n-\frac{1}{2}}\left(i-\frac{1}{2},j,k+\frac{1}{2}\right)}{\Delta_x}\right.$$
$$\left.-\frac{H_x^{n-\frac{1}{2}}\left(i,j+\frac{1}{2},k+\frac{1}{2}\right)-H_x^{n-\frac{1}{2}}\left(i,j-\frac{1}{2},k+\frac{1}{2}\right)}{\Delta_y}\right] \tag{A5}$$

$$E_z^n\left(i,j,k+\frac{1}{2}\right)=$$
$$\frac{2\varepsilon_0-\Delta_t\sigma_y\left(i,j,k+\frac{1}{2}\right)}{2\varepsilon_0+\Delta_t\sigma_y\left(i,j,k+\frac{1}{2}\right)}\cdot E_z^{n-1}\left(i,j,k+\frac{1}{2}\right)$$
$$+\frac{2\varepsilon_0+\Delta_t\sigma_z\left(i,j,k+\frac{1}{2}\right)}{2\varepsilon_0^2\varepsilon_z+\Delta_t\varepsilon_0\varepsilon_z\sigma_y\left(i,j,k+\frac{1}{2}\right)}\cdot D_z^n\left(i,j,k+\frac{1}{2}\right)$$
$$-\frac{2\varepsilon_0-\Delta_t\sigma_z\left(i,j,k+\frac{1}{2}\right)}{2\varepsilon_0^2\varepsilon_z+\Delta_t\varepsilon_0\varepsilon_z\sigma_y\left(i,j,k+\frac{1}{2}\right)}\cdot D_z^{n+1}\left(i,j,k+\frac{1}{2}\right) \tag{A6}$$

$$B_z^{n+\frac{1}{2}}\left(i+\frac{1}{2},j+\frac{1}{2},k\right)=$$
$$\frac{2\varepsilon_0-\Delta_t\rho_x\left(i+\frac{1}{2},j+\frac{1}{2},k\right)}{2\varepsilon_0+\Delta_t\rho_x\left(i+\frac{1}{2},j+\frac{1}{2},k\right)}\cdot B_z^{n-\frac{1}{2}}\left(i+\frac{1}{2},j+\frac{1}{2},k\right)$$
$$-\frac{1}{2\varepsilon_0+\Delta_t\rho_x\left(i+\frac{1}{2},j+\frac{1}{2},k\right)}\cdot$$
$$\left[\frac{E_y^n\left(i+1,j+\frac{1}{2},k\right)-E_y^n\left(i,j+\frac{1}{2},k\right)}{\Delta_x}\right.$$
$$\left.-\frac{E_x^n\left(i+\frac{1}{2},j+1,k\right)-E_x^n\left(i+\frac{1}{2},j,k\right)}{\Delta_y}\right] \tag{A7}$$

$$H_z^{n+\frac{1}{2}}\left(i+\frac{1}{2},j+\frac{1}{2},k\right)=$$
$$\frac{2\varepsilon_0-\Delta_t\rho_y\left(i+\frac{1}{2},j+\frac{1}{2},k\right)}{2\varepsilon_0+\Delta_t\rho_y\left(i+\frac{1}{2},j+\frac{1}{2},k\right)}\cdot H_z^{n-\frac{1}{2}}\left(i+\frac{1}{2},j+\frac{1}{2},k\right)$$
$$+\frac{2\varepsilon_0+\Delta_t\rho_z\left(i+\frac{1}{2},j+\frac{1}{2},k\right)}{2\varepsilon_0\mu_0\mu_z+\Delta_t\mu_0\mu_z\rho_y\left(i+\frac{1}{2},j+\frac{1}{2},k\right)}$$
$$\cdot B_z^{n+\frac{1}{2}}\left(i+\frac{1}{2},j+\frac{1}{2},k\right)$$
$$-\frac{2\varepsilon_0-\Delta_t\sigma_z^{H_z}\left(i+\frac{1}{2},j+\frac{1}{2},k\right)}{2\varepsilon_0\mu_0\mu_z+\Delta_t\mu_0\mu_z\rho_y\left(i+\frac{1}{2},j+\frac{1}{2},k\right)}$$
$$\cdot B_z^{n-\frac{1}{2}}\left(i+\frac{1}{2},j+\frac{1}{2},k\right) \tag{A8}$$

ACKNOWLEDGMENT

The authors are very grateful to Prof. S. Wei of Zhejiang University for his valuable advice on numerical stability study of FDTD.

REFERENCES

[1] L. Tsang, E. Njoku, and J. A. Kong, "Microwave thermal emission from a stratified medium with nonuniform temperature distribution," *J. Appl. Phys.*, vol. 46, no. 12, pp. 5127–5133, Dec. 1975.
[2] P. E. Wannamaker, G. W. Hohmann, and W. A. SanFilipo, "Electromagnetic modeling of three-dimensional bodies in layered earths using integral equations," *Geophysics*, vol. 49, no. 1, pp. 60–74, Jan. 1982.
[3] A. Karlsson and G. Kristensson, "Electromagnetic scattering from subterranean obstacles in a stratified ground," *Radio Sci.*, vol. 18, no. 3, pp. 345–356, May 1983.
[4] P. S. Hall, "Probe compensation in thick microstrip patches," *Electron. Lett.*, vol. 23, no. 11, pp. 606–607, May 1987.
[5] S. D. Targonski, R. B. Waterhouse, and D. M. Pozar, "Design of wide-band aperture-stacked patch microstrip antennas," *IEEE Trans. Antennas Propag.*, vol. 46, no. 9, pp. 1245–1251, Sep. 1998.
[6] A. Corcoran, L. Sexton, and B. Seaman, "The laser drilling of multilayer aerospace material systems," *J. Mater. Process. Technol.*, vol. 123, pp. 100–106, Apr. 2002.
[7] E. Kostson and P. Fromme, "Fatigue crack growth monitoring in multilayered structures using guided ultrasonic waves," *J. Phys., Conf. Ser.*, vol. 195, no. 1, 2009, Art. no. 012003.
[8] B. Kursuncu, H. Caliskan, P. Panjan, and S. Y. Guven, "Wear behavior of multilayer nanocomposite TiAlSiN/TiSiN/TiAlN coated carbide cutting tool during face milling of inconel 718 superalloy," *J. Nano Res.*, vol. 47, pp. 11–16, May 2017.
[9] M.-J. Tsai, F. De Flaviis, O. Fordham, and N. G. Alexopoulos, "Modeling planar arbitrarily shaped microstrip elements in multilayered media," *IEEE Trans Microw. Theory Techn.*, vol. 45, no. 3, pp. 330–337, Mar. 1997.
[10] R.-C. Hsieh and J.-T. Ku, "Fast full-wave analysis of planar microstrip circuit elements in stratified media," *IEEE Trans Microw. Theory Techn.*, vol. 46, no. 9, pp. 1291–1297, Sep. 1998.
[11] W. Zhang, "Modeling and analysis for pulsed terahertz nondestructive testing of hidden corrosion," *Chin. J. Nondestruct. Test.*, vol. 31, no. 10, pp. 790–795, Oct. 2009.
[12] P.-P. Ding, C.-W. Qiu, S. Zouhdi, and S. P. Yeo, "Rigorous derivation and fast solution of spatial-domain green's functions for uniaxial anisotropic multilayers using modified fast Hankel transform method," *IEEE Trans. Microw. Theory Techn.*, vol. 60, no. 2, pp. 205–217, Feb. 2012.
[13] Y. Zhong, P. P. Ding, M. Lambert, D. Lesselier, and X. Chen, "Fast calculation of scattering by 3-D inhomogeneities in uniaxial anisotropic multilayers," *IEEE Trans. Antennas Propag.*, vol. 62, no. 12, pp. 6365–6374, Dec. 2014.
[14] V. R. Melapudi, L. Udpa, S. S. Udpa, and W. P. Winfree, "Ray tracing model for terahertz inspection of spray on foam insulation (SOFI)," in *Proc. 12th Biennial IEEE Conf. Electromagn. Field Comput.*, Miami, FL, USA, Apr./May 2006, p. 421.
[15] J. Schneider and S. Hudson, "A finite-difference time-domain method applied to anisotropic material," *IEEE Trans. Antennas Propag.*, vol. 41, no. 7, pp. 994–999, Jul. 1993.
[16] J. B. Verdu, R. Gillard, J. Citerne, and K. Moustadir, "An extension of the PML technique to the FDTD analysis of multilayer planar circuits and antennas," *Microw. Opt. Technol. Lett.*, vol. 10, pp. 323–327, Dec. 1995.
[17] M. S. Sarto, "Sub-cell model of multilayer composite materials for full FDTD and hybrid MFIE/FDTD analyses," in *Proc. IEEE Int. Symp. Electromagn. Compat.*, vol. 2, Aug. 2002, pp. 737–742.
[18] H. Zhang, W.-Y. Yin, Z. G. Zhao, H. Zhou, Y. Liao, and X. Meng, "Fast Simulation of multilayered anisotropic carbon fiber composite thin layers using the embedded thin layer model and improved FDTD suitable for high performance computing," in *Proc. IEEE Int. Symp. Antenna, Propag. EM Theory (ISAPE)*, Dec. 2018, pp. 1–4.
[19] C. D. Moss, F. L. Teixeira, and J. A. Kong, "Analysis and compensation of numerical dispersion in the FDTD method for layered, anisotropic media," *IEEE Trans. Antennas Propag.*, vol. 50, no. 9, pp. 1174–1184, Sep. 2002.
[20] T. Yasui, T. Yasuda, T. Araki, and K. I. Sawanaka, "Terahertz paintmeter for noncontact monitoring of thickness and drying progress in paint film," *Appl. Opt.*, vol. 44, pp. 6849–6856, Nov. 2005.
[21] R. F. Anastasi and E. I. Madaras, "Terahertz NDE for under paint corrosion detection and evaluation," in *Proc. AIP Conf.*, vol. 820, Mar. 2006, pp. 49–56.
[22] T. Fukuchi, N. Fuse, and M. Okada, "Measurement of refractive index and thickness of topcoat of thermal barrier coating by reflection measurement of terahertz waves," *IEEE Trans. Fundam. Mater.*, vol. 96, no. 12, pp. 37–45, Dec. 2013.
[23] D. K. Hsu, K. S. Lee, Y.-D. Woo, K.-H. Im, and J. W. Park, "NDE inspection of terahertz waves in wind turbine composites," *Int. J. Precis. Eng. Manuf.*, vol. 13, pp. 1183–1189, Jul. 2012.
[24] T. Chady and P. Lopato, "Testing of glass-fiber reinforced composite materials using terahertz technique," *Int. J. Appl. Electromagn. Mech.*, vol. 33, pp. 1599–1605, Jan. 2010.
[25] J.-P. Berenger, "Three-dimensional perfectly matched layer for the absorption of electromagnetic waves," *J. Comput. Phys.*, vol. 127, no. 2, pp. 363–379, Sep. 1996.

HUILING HU received the B.E. degree from Weifang University, Weifang, China, in 2015. She is currently pursuing the M.S. degree in electromagnetic field and microwave technology with Fudan University, Shanghai, China. Her current research focus is on computational electromagnetics, e.g., numerical modeling and simulation for scattering from multilayer composites and terahertz wave propagation.

HONGXIA YE (M'07) received the B.S. and M.S. degrees from Xi'an Jiaotong University, Xi'an, China, in 2000 and 2003, respectively, and the Ph.D. degree from Fudan University, Shanghai, China, in 2007. She is currently an Associate Professor with the School of Information Science and Engineering, Fudan University. She has published over 70 articles in China and abroad. Her research interests include computational electromagnetics, e.g., numerical modeling and simulation for scattering from rough surfaces and volumetric objects, and automatic target recognition for synthetic aperture radar technology. She was a recipient of the First Grade Science Prize of MoE, in 2009.

YA-QIU JIN (SM'89–F'04) received the M.S., E.E., and Ph.D. degrees from the Massachusetts Institute of Technology, Cambridge, MA, USA, in 1982, 1983, and 1985, respectively. He is currently the Te-Pin Professor of the Key Laboratory for Information Science of Electromagnetic Waves (MoE), Fudan University, Shanghai, China. He is also an Academician with the Chinese Academy of Sciences. He has published more than 680 articles in refereed journals and conference proceedings and 14 books. His main research interests include polarimetric scattering and radiative transfer in complex natural media, microwave remote sensing, as well as applications in Earth terrain and planetary surfaces, and computational electromagnetics. He has been an IEEE GRSS Distinguished Speaker, since 2010. He is also an Associate Editor of IEEE Access.